Neurobiology of Disease 38 (2010) 125–135

Contents lists available at ScienceDirect

Neurobiology of Disease

journal homepage: www.elsevier.com/locate/ynbdi

Neuromuscular defects and breathing disorders in a new mouse model of spinal muscular atrophy

Magali Michaud [a], Thomas Arnoux [a], Serena Bielli [a], Estelle Durand [b], Yann Rotrou [b], Sibylle Jablonka [c], Fabrice Robert [a], Marc Giraudon-Paoli [a], Markus Riessland [d], Marie-Geneviève Mattei [e], Emile Andriambeloson [f], Brunhilde Wirth [d], Michael Sendtner [c], Jorge Gallego [b], Rebecca M. Pruss [a], Thierry Bordet [a,*]

[a] Trophos, Parc Scientifique de Luminy, Luminy Biotech Entreprise, Case 931, 13288 Marseille, France
[b] Inserm UMR 676, Université Paris 7, Hôpital Robert Debré, Paris, France
[c] Institute of Clinical Neurobiology, University of Wuerzburg, Zinklesweg 10, 97078 Würzburg, Germany
[d] Institute of Human Genetics, Institute of Genetics and Center for Molecular Medicine Cologne, University of Cologne, Kerpener Str. 34, 50931 Cologne, Germany
[e] Inserm UMR 910, Université de la Méditerranée, Faculté de Médecine de la Timone, Marseille, France
[f] Neurofit, Parc d'Innovation, Illkirch, France

ARTICLE INFO

Article history:
Received 17 November 2009
Revised 7 January 2010
Accepted 11 January 2010
Available online 18 January 2010

Keywords:
Spinal muscular atrophy
Motor neuron disease
Mouse model
Survival motor neuron gene
Neurodegeneration
Behavior
Breathing disorders
Neuromuscular junction
Development

ABSTRACT

Spinal muscular atrophy (SMA) is caused by insufficient levels of the survival motor neuron (SMN) protein leading to muscle paralysis and respiratory failure. In mouse, introducing the human *SMN2* gene partially rescues *Smn*$^{-/-}$ embryonic lethality. However current models were either too severe or nearly unaffected precluding convenient drug testing for SMA. We report here new *SMN2*;*Smn*$^{-/-}$ lines carrying one to four copies of the human *SMN2* gene. Mice carrying three *SMN2* copies exhibited an intermediate phenotype with delayed appearance of motor defects and developmental breathing disorders reminiscent of those found in severe SMA patients. Although normal at birth, at 7 days of age respiratory rate was decreased and apnea frequency was increased in SMA mice in parallel with the appearance of neuromuscular junction defects in the diaphragm. With median survival of 15 days and postnatal onset of neurodegeneration, these mice could be an important tool for evaluating new therapeutics.

Introduction

Proximal spinal muscular atrophy (SMA) is the second most frequent autosomal recessive genetic disease in humans with an incidence of approximately 1 in 6000 births (McAndrew et al., 1997; Pearn, 1978; Scheffer et al., 2001) and a carrier frequency varying from 1 in 37 persons in the European population and up to 1:125 among other ethnicities (Feldkotter et al., 2002; Hendrickson et al., 2009). SMA is characterized by selective degeneration and loss of spinal motor neurons leading to progressive muscle weakness and respiratory failure (Crawford and Pardo, 1996; Schroth, 2009). SMA is caused by the homozygous loss of the telomeric copy of the survival motor neuron gene (*SMN1*) on human chromosome 5q13 (Bussaglia et al., 1995; Lefebvre et al., 1995). The severity of the disease is modified by the number of centromeric *SMN2* copies, milder forms having the highest number of *SMN2* copies (Burghes, 1997; Coovert et al., 1997; Feldkotter et al., 2002; Lefebvre et al., 1997). *SMN1* produces a full-length transcript whereas *SMN2* generates mostly a transcript lacking exon 7 that is translated into an unstable and rapidly degraded SMNΔ7 protein (Le et al., 2000; Lorson and Androphy, 2000; Lorson et al., 1998, 1999; Monani et al., 1999). The SMN protein is involved in several processes including pre-messenger RNA splicing, transcription and metabolism of ribosomal RNA, and axonal transport of mRNA (Carrel et al., 2006; Liu and Dreyfuss, 1996; Liu et al., 1997; Pellizzoni et al., 1998, 2002; Rossoll et al., 2003; Zhang et al., 2003). However, the molecular pathway linking SMN deficit to SMA phenotype remains unclear. Despite the widespread expression of SMN in various tissues, motor neurons are predominantly affected suggesting that SMN may regulate a specific function in motor neurons (see recent review in Burghes and Beattie, 2009). Modeling SMA in animal models is thus crucial to further understand disease pathogenesis, SMN function and to test potential therapies.

* Corresponding author. Fax: +33 491 828 289.
E-mail address: tbordet@trophos.com (T. Bordet).
Available online on ScienceDirect (www.sciencedirect.com).

0969-9961/$ – see front matter © 2010 Elsevier Inc. All rights reserved.
doi:10.1016/j.nbd.2010.01.006

In the mouse genome, there is one *Smn* gene (DiDonato et al., 1997; Viollet et al., 1997) and its deletion results in embryonic lethality (Frugier et al., 2000; Hsieh-Li et al., 2000; Schrank et al., 1997). Its specific deletion in neurons led to an SMA phenotype with progressive motor defects and neuromuscular junction alterations suggestive of a 'dying-back' degenerative process in SMA (Cifuentes-Diaz et al., 2002; Frugier et al., 2000). Other models have been developed introducing the human *SMN2* transgene onto the null $Smn^{-/-}$ background (SMA mice). While SMA mice carrying one or two copies of the human *SMN2* transgene display a very severe phenotype and die shortly after birth (Hsieh-Li et al., 2000; Monani et al., 2000), mice carrying higher copy numbers (8–16 copies) were fully rescued (Monani et al., 2000). Thus disease severity in mice, as in patients, depends on a fine tuning of SMN protein expression. Severe SMA pathology in mice was partly rescued when *SMN2* was introduced along with neighboring genomic DNA including part of the neuronal apoptosis inhibitory protein (*NAIP*) gene and the full length small EDRK-rich factor 1 (*SERF1*) gene (Tsai et al., 2006, 2008a,b). Similarly, introduction of a known *SMN1* missense mutation (A2G) in SMA mice carrying one copy of *SMN2* resulted in a very mild phenotype with slowly progressive motor neuron degeneration and enhanced lifespan (Monani et al., 2003). In contrast, SMNΔ7 only poorly rescued SMA mice, extending survival from 5 to 13 days (Le et al., 2005). Although these models provided evidence that milder SMA phenotypes could be generated on a null *Smn* background, they do not reproduce the genetics found in patients, limiting their value for testing potential therapeutics.

We addressed this challenge by generating new *SMN2*;$Smn^{-/-}$ lines on a pure C57BL/6N background with *SMN2* transgene copy number ranging from 1 to 4. SMA mice carrying three copies of *SMN2* displayed marked defects in neuromuscular junction development, especially in the diaphragm. These defects correlated with the development of manifest breathing defects that could be responsible for premature death of SMA mice. Though still severely afflicted, this new SMA mouse is the longest surviving SMA mouse model described to date produced by introducing *SMN2* alone onto a pure genetic background. The delayed onset of neurodegeneration in this model should facilitate further advancement of SMA pathophysiology and testing potential therapies.

Materials and methods

Generation of SMN2 transgenic mice and breeding strategy

SMN2 transgenic lines, N11 and N46, were generated according to previously described procedures (Monani et al., 2000). Briefly PAC 215P15 was digested with *Bam*HI and *Cla*I to excise a 35.5 kb fragment encompassing the *SMN2* gene sequence. This fragment was injected into fertilized FVB mouse oocytes. Eight founders out of 13 transgenic animals were obtained. The copy number was first estimated by Southern blot of tail DNA. Selected mice were crossed with $Smn^{+/-}$ mice (Schrank et al., 1997) obtained from Dr. Michael Sendtner (University of Wurzburg, Germany) and backcrossed to C57BL6/N for at least 10 generations to obtain a pure genetic background. Transgenic $SMN2(N11)^{+/-}$;$Smn^{+/-}$ were interbred (F0) to generate homozygous $SMN2(N11)^{+/+}$;$Smn^{+/-}$ mice [F1; B6.Cg-Tg (SMN2)11Tro $Smn1^{tm1Msd}$/N, stock number: #008629 at the Jackson Laboratory). The same strategy was used to obtain $SMN2(N46)^{+/+}$; $Smn^{+/-}$ mice [B6.Cg-Tg(SMN2)46Tro $Smn1^{tm1Msd}$/N, stock number: #008630 at the Jackson Laboratory]. N11/N46 SMA mice [$SMN2(N11)^{+/-}$; $SMN2(N46)^{+/-}$;$Smn^{-/-}$] were obtained by breeding male $SMN2(N11)^{+/+}$;$Smn^{+/-}$ with female $SMN2(N46)^{+/+}$;$Smn^{+/-}$ mice. Offspring were genotyped using a PCR-based assay on tail DNA. The mouse *Smn* knock-out allele was detected using the primers 5′-CTTGGGTGGAGAGGCTATTC-3' and 5′-AGGTGAGATGACAGGAGATC-3', and the wild-type allele with the primers 5′-TTTTCTCCCTCTTCAGAGTGAT-3′ and 5′-CTGTTTCAAGGGAGTTGTGGC-3′. PCR conditions were: 3 min 94°C heating step, followed by 35 cycles of 94°C for 30 s, 62°C for 1 min, 72°C for 1 min, and 2 min at 72°C.

Animals were maintained in environment-controlled rooms in individual ventilated cages. All the experiments were performed in accordance with institutional guidelines (French Ministry of Agriculture, Agreement No. 13.055.15 for Trophos animal facility).

Quantitative real-time PCR of SMN2 transgene copy numbers

Genomic tail-tip DNA was isolated and purified using the ChargeSwitch® gDNA Mini Tissue Kit (Invitrogen) according to the manufacture's protocol. DNA concentration was determined using Quant-iT™ PicoGreen® dsDNA Kit (Invitrogen). The DNA concentration was adjusted to 40 ng/μl (in TE buffer) and for homogenous dissolution incubated on a laboratory shaker (HLC) at 37°C at 600 rpm for 1 h. Afterwards DNA concentration was again measured (see above) and adjusted to 5 ng/μl. Following the repetition of the homogenization step the exact DNA concentration was verified by a SYBR green real-time PCR (Power-SYBR® green, Applied Biosystems) for the murine single-copy gene apoliprotein B (*ApoB*). Primers for this internal control were chosen as follows, *ApoB* forward primer: 5′-CACGTGGGCTCCAGCATT-3′; *ApoB* reverse primer: 5′-TCACCAGTCATTTCTGCCTTTG-3′ (adapted from Lobsiger et al. 2009). Finally, the *SMN2* copy number was determined using a LightCycler® 1.5 real-time PCR system (Roche). For this purpose 15 ng of genomic DNA was used in each real-time PCR reaction. The quantification was performed with the help of a standard curve of DNA with a known *SMN2* copy number according to a protocol described previously (Feldkotter et al., 2002).

Western blotting analysis

Tissue samples from 5 day-old animals (PND5) were lysed in RIPA buffer (150 mM NaCl, 50 mM Tris, 1% NP40, 0.5% Sodium Desoxycholate) supplemented with proteinase inhibitors (Complete EDTA-free, Roche). Protein concentrations were determined using the BCA Protein Assay kit (Pierce, Rockford, IL). Proteins (30 μg) were electrophoresed on pre-cast 12% polyacrylamide gel (Invitrogen) and transferred to nitrocellulose membranes (BIORAD). SMN was detected with an anti-SMN antibody (BD Transduction Laboratories) at a 1:1000 dilution in TBS-0.1% tween-5% milk powder, while tubulin was detected using a 1:1000 dilution of the anti-tubulin antibody (Sigma) in TBS-tween-milk. The primary antibodies were then detected with a species-specific antibody conjugated to horseradish peroxidase (Pierce) and visualized using West Dura chemiluminescent reagent (Pierce).

Histological analysis of spinal motor neurons, motor axons and muscle

Mice were deeply anesthetized and transcardially perfused with 1× Sorensen's phosphate buffer followed with 4% paraformaldehyde (PFA). L1–L6 spinal cord segments were dissected at post-natal days 1 and 15 and processed as previously described (Monani et al., 2003). The sciatic nerves (ventral roots from L4 to L6) were fixed overnight with 4% PFA in Sorenson's buffer at 4°C. The distal phrenic nerves were harvested on deeply anesthetized mice, fixed with 4% PFA and 2.5% glutaraldehyde before dissection and for an extra night at 4°C. Each nerve sample was post-fixed in 1% osmium tetroxide in Sorenson's buffer overnight at room temperature, dehydrated in serial alcohol solutions, and embedded in Epon. Cross sections (1-μm thick) were prepared and stained with 1% toluidine blue. Axonal counting was performed on ventral root of the nerve section using a semi-automated digital image processing program (Image J). Morphological analysis was performed only on fibers considered as non-degenerated. Histology of the gastrocnemius was performed on

unfixed samples from 8 and 15 day-old control or transgenic mice. Transverse muscle sections (20-μm thick) were stained with eosin and hematoxylin. Gastrocnemius muscle fiber areas were outlined using an adapted tool from Image J and then manually corrected before surface area measurement.

All quantifications were performed blind regarding the genotype on a minimum of five animals of each genotype and age. Data were analyzed using GraphPad Prism software. Statistical comparison was performed using Student's *t*-test.

Immunohistochemical analysis of neuromuscular junctions (NMJs)

NMJs in the diaphragm were analyzed in whole-mount preparations. Tissues were prepared from 1, 8 and 15 day-old mice. Animals were perfused with 2% paraformaldehyde, and then muscles were dissected and tissues post-fixed with 2% paraformaldehyde overnight at 4°C then incubated for at least 2 h in PBS (pH 7.4) containing 0.1 M glycine. Muscles were permeabilized in PBS, 4% bovine serum albumin (BSA), 0.5% Triton X-100, overnight at 4°C. Antibody incubation was carried out in the blocking/permeabilization solution at room temperature for 6 h. NMJs in gastrocnemius muscle were analyzed on 35-μm thick cryosections. Fresh tissues were fixed in 4% paraformaldehyde and cryopreserved in 20% sucrose. Cryosections were permeabilized in PBS, 5% BSA, 0.5% Triton X-100 for 1h30 at 37°C. Primary and secondary antibodies were diluted in PBS, 1% BSA, 0.25% Triton X-100 and incubations were for 2 h and 1h30 respectively at room temperature. Both for the whole-mount staining and for cryosections the pre-synaptic motor nerve terminals were stained with polyclonal rabbit antibody directed against the 145 kDa isoform of neurofilament, neurofilament M (used at 1:1000; Millipore) and the synaptic vesicles with mouse monoclonal anti-SV2 antibody (used at 1:200; Developmental Studies Hybridoma Bank). Post-synaptic nicotinic acetylcholine receptors (AChRs) were labeled with Alexa 647- or rhodamine-conjugated α-bungarotoxin (used at 1:1000; Invitrogen). Confocal images were acquired using a Zeiss LSM 510 inverted microscope.

EMG

Electrophysiological recordings were performed on 15 day-old mice using a KEYPOINT electromyograph (Medtronic, Boulogne-Billancourt, France). Mice were anaesthetized by intraperitoneal injection of 100 mg/kg ketamine chlorhydrate (Imalgene 500®, Rhône Mérieux, Lyon, France) and 1.6 mg/kg xylazine (Rompum® 2%, Bayer Pharma, Kiel, Germany). Normal body temperature was carefully maintained with a heating lamp and monitored by a contact thermometer (Quick, Bioblock Scientific, Illkirch, France) placed on the tail surface. Compound action potentials (CMAP) of the calf muscles were elicited by single 0.2 ms supramaximal stimulation (12.8 mA) of the sciatic nerve at the sciatic notch through noninsulated platinum needle electrodes and were recorded between two electrodes placed over the belly of the anterior tibial muscle and at the ankle. Shape and amplitude of the potentials did not change when the recording electrode was moved to the gastrocnemius muscle; this indicated that the recorded potential was the combined extensor and flexor muscle potential. Peak-to-peak amplitudes (mV), the motor latencies (ms) and the duration (time needed between depolarization and repolarization session) were measured.

Behavioral testing

The spontaneous righting reflex was evaluated in mouse pups from PND2 to PND8. Mice were placed on their backs and their ability to reposition themselves dorsal side up was assessed over a 30 s period. Each pup was tested twice with a 1.5 min recovery period between tests.

Negative geotaxis test was adapted from El-Khodor et al. (2008) from PND4 to PND12. Briefly, pups were placed on an inclined plane (45°) with the head facing down. The pup's ability to perform in this test was scored from 0 to 4 as follows: 0, failed to perform the test and fell from the plane; 1, unable to turn but able to stay on the plane; 2, able to turn to a maximum of 90° then either stop or fall; 3, able to turn around 180° then either stop or fall; 4, able to turn 180° and to climb upwards. Each pup was tested twice with a 1.5 min recovery period between tests. The time to complete the task was recorded over a 60 s period. For mice that failed to orient themselves, the time was recorded as 60 s.

Thermal hyperalgesia was assessed at PND15 by placing the mice into a glass cylinder located on a hot plate adjusted to 52°C. The latency to the first reaction was recorded (paw lifting or licking) with a cut off time of 30 s.

Measurement of respiratory parameters using plethysmography

Breathing variables were measured noninvasively on 1 and 7 day old mice. All mice in a litter were evaluated prior to genotyping then data were analyzed by genotype. Testing was performed under normoxic conditions and in responses to hypoxia using a battery of three whole-body flow barometric plethysmographs previously described (Dauger et al., 2004; Ramanantsoa et al., 2006). Briefly, plethysmograph chambers were immersed in a thermoregulated water-bath maintaining animal temperature at 33°C, which corresponds to thermoneutrality in newborn rodents. After 15-min normoxia, hypoxia was achieved by switching the airflow to 10% O_2 + 90% N_2 at the same flow rate (200 ml/min per chamber) for 3 min, after which the flow was switched back to normoxia for 12 min (total duration of the session: 30 min). Breath duration (T_{TOT}, s), tidal volume (V_T, μl g^{-1}), and minute ventilation (V_E, calculated as V_T/T_{TOT} and expressed in μl s^{-1} g^{-1}) were calculated on apnea-free periods (see apnea determination below). Breath-by-breath values for V_E, V_T, and T_{TOT} were averaged over consecutive 30-s periods. The baseline (i.e. normoxic) levels for these variables in each test were calculated as the mean value over the 3-min of air-breathing preceding the hypoxic exposure. The peak V_E during hypoxia was determined 90-s after the hypoxic onset. This peak-value was calculated as the mean value over 1-min period to take into account possible interindividual differences in time to reach the peak response to hypoxia. The V_E response to hypoxia was expressed as the percentage V_E change relative to baseline average V_E, using the formula $100 \cdot x$(peak V_E - baseline V_E)/baseline V_E. Apneas were defined as ventilatory pauses longer than twice the duration of the preceding breath (Sawnani et al., 2004) and determined using an automatic classification method based on spectral analysis (Matrot et al., 2005). Total apnea duration was calculated over successive 30-s periods. Breathing variables were subjected to standard repeated measures analyses of variance with genotype as a between-subjects factors and period (Normoxia, Hypoxia, Post-Hypoxia) as a repeated factor. The ventilatory response to hypoxia, expressed as the percentage VE change relative to baseline was subjected to standard ANOVAs with genotype as a between-subject factor. All statistical analyses were conducted using Statview 5 (Abacus Concepts, Berkeley, CA).

Results

New SMN2 transgenic lines on a null Smn background

Two new human *SMN2* transgenic mouse lines were generated; the N11 line carrying one copy of *SMN2* on chromosome 18, and the N46 line carrying two *SMN2* copies at a single insertion site on chromosome 3 (Table 1 and Supplementary material, Fig. S1). These mice were crossed with $Smn^{+/-}$ mice and backcrossed to C57BL/6N for more than 10 generations. On a null *Smn* background, N11 mice hemizygous for the *SMN2* transgene (one *SMN2* copy) displayed an embryonic lethality, while homozygous mice (two *SMN2* copies),

Table 1
Quantitative real-time PCR analysis of *SMN2* copy number in different transgenic mouse lines ($n=3$–4/genotype): N11 [*SMN2(N11)*$^{+/+}$;*Smn*$^{+/-}$], N46 [*SMN2(N46)*$^{+/+}$; *Smn*$^{+/-}$] and N11/N46 [*SMN2(N11)*$^{+/-}$;*SMN2(N46)*$^{+/-}$;*Smn*$^{+/-}$].

Line	No. of SMN2 copies	Minimum/maximum average values	Mean ± SD	CV (%)
N11	2	1.6/2.3	1.9 ± 0.1	7.6
N46	4	3.3/4.4	3.9 ± 0.2	4.7
N11/N46	3	2.2/3.2	2.7 ± 0.1	5.1

hereafter referred to as N11 SMA mice [*SMN2(N11)*$^{+/+}$;*Smn*$^{-/-}$], exhibit a severe phenotype with median survival around 6 days after birth (Figs. 1A and B). Though indistinguishable from control littermates at birth, N11 SMA pups rapidly start losing weight after the first 48 h and die within a few days. Similarly, N46 mice hemizygous for the *SMN2* transgene (two copies) displayed an embryonic lethality on a null *Smn* background. When homozygous for the transgene (four copies) N46 mice on a null *Smn* background, hereafter referred as N46 SMA mice [*SMN2(N46)*$^{+/+}$; *Smn*$^{-/-}$], were viable, fertile and did not display evident SMA-like phenotype. However, adult mice exhibited progressive degeneration at their extremities, shortening and loss of their tails, external ear tissue and swollen hind paws; their body weight gain was also slightly slowed compared to control mice (Figs. 1A and D) although their lifespan is not shorter than control mice. These observations indicate that two copies of *SMN2* transgene were not sufficient to rescue the SMA phenotype whereas four copies nearly fully rescued the *Smn* knockout phenotype on a C57B6/N genetic background.

Characterization of mildly affected SMA mice (N11/N46 SMA)

Since N11 SMA mice (two copies of *SMN2*) were too severely afflicted and N46 SMA mice (four copies of *SMN2*) were nearly fully rescued, neither line provides a convenient model for studying SMA pathophysiology or testing potential therapeutics. In order to produce an intermediate phenotype, we crossed male *SMN2(N11)*$^{+/+}$;*Smn*$^{+/-}$ and female *SMN2(N46)*$^{+/+}$;*Smn*$^{+/-}$ with the hope of generating mildly affected SMA animals. As expected, double heterozygotes *SMN2(N11)*$^{+/-}$;*SMN2(N46)*$^{+/-}$ on a null *Smn* background (hereafter referred as N11/N46 SMA mice) carried three copies of *SMN2* (Table 1) and expressed intermediate SMN protein levels in various tissues compared to N11 SMA mice and N46 SMA mice at same age (Fig. 2D). Interestingly particularly low SMN protein levels were observed in gastrocnemius muscle and in heart when compared with wild-type mice while levels in spinal cord and brain were comparatively less reduced.

N11/N46 SMA mice displayed a milder phenotype compared to N11 SMA mice (Fig. 2). In the first 4 days N11/N46 SMA mice were indistinguishable from control littermates [*SMN2(N11)*$^{+/-}$;*SMN2 (N46)*$^{+/-}$; *Smn*$^{+/-}$ and *SMN2(N11)*$^{+/-}$;*SMN2(N46)*$^{+/-}$*Smn*$^{+/+}$] after which they started to show a significantly diminished weight gain (Figs. 2A, C). By 9 days, signs of muscle weakness were evident and worsened over the following week. At day 14, mice still surviving displayed an abnormal gait. N11/N46 SMA mice survived for an average of 15.2 ± 0.4 days (mean ± SEM; $n=202$) with a median survival of 14 days. No difference in gender was observed (data not shown). Surprisingly a few animals (9 out of 211) escaped death and reached adulthood without evident phenotype with the exception of feet, tail and ear pathology (Figs. 2A and B). Inversing the breeding by crossing female *SMN2(N11)*$^{+/+}$;*Smn*$^{+/-}$ and male *SMN2(N46)*$^{+/+}$; *Smn*$^{+/-}$ resulted in a slightly different phenotype with increased lifespan (median survival of 22 days; $n=106$) and a higher percentage of animals escaping death (26 out of 106 mice survived beyond 100 days). Quantitative PCR analysis on these "long survivors" showed no change in *SMN2* copy numbers compared with affected mice (data not shown). This suggests that epigenetic factors may modify disease progression and survival.

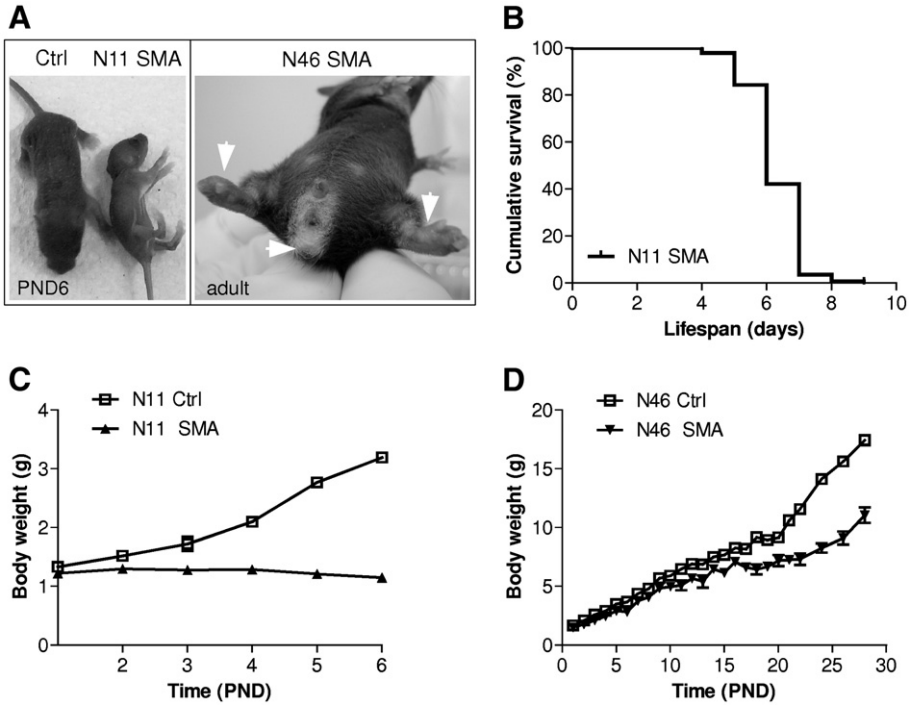

Fig. 1. Phenotypic characteristics of N11 SMA mice and N46 SMA mice. (A) Representative pictures of a N11 SMA mouse [*SMN2(N11)*$^{+/+}$;*Smn*$^{-/-}$] compared to control littermate [*SMN2(N11)*$^{+/+}$;*Smn*$^{+/+}$] at PND6, and of adult N46 SMA mice [*SMN2(N46)*$^{+/+}$;*Smn*$^{-/-}$]. Arrows indicate typical phenotypic characteristics of adult N46 SMA mice including edematous hind paws and shortened or absent tail as previously described for other SMA mice (Hsieh-Li et al., 2000; Tsai et al., 2006). (B) Kaplan–Meier survival curves of N11 SMA mice ($n=140$). (C, D) Body weight evolution in N11 SMA mice and N46 SMA mice compared to control littermates (mean ± SEM; $n=2$–58 for each time point). The two-way ANOVA test indicated a significant difference (Bonferroni posttest, $P<0.05$) between body weight of SMA and control mice from PND2 and PND10 onward for N11 SMA mice and N46 SMA mice, respectively.

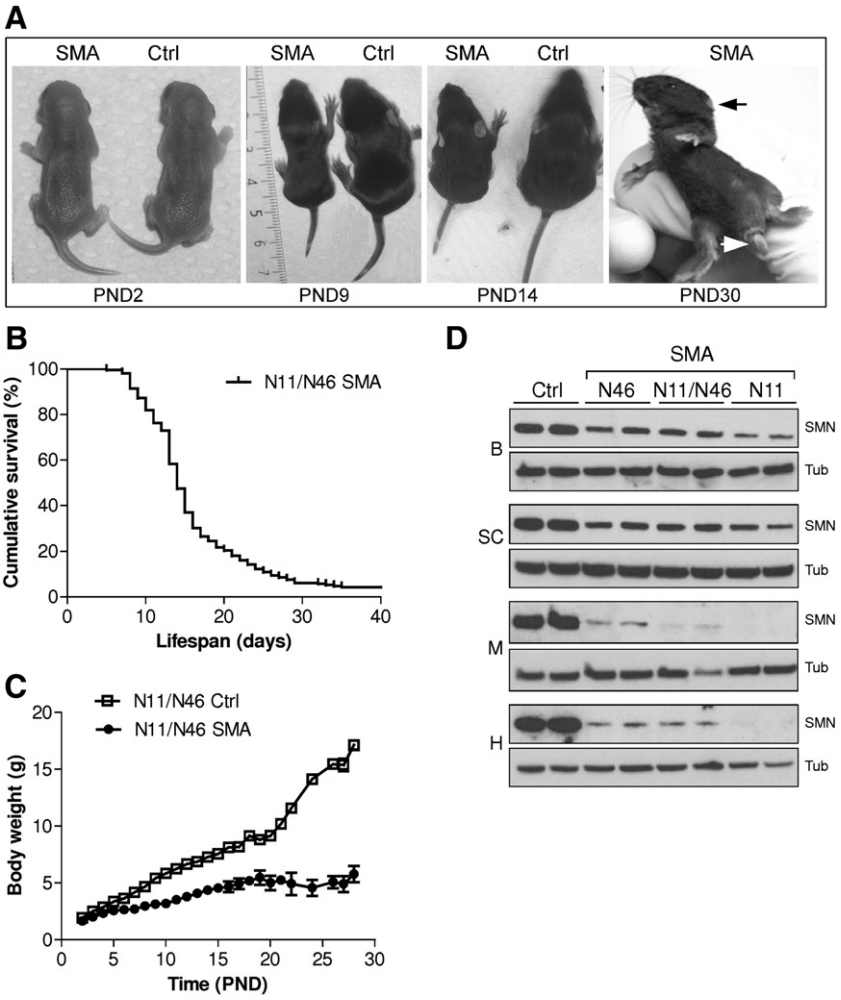

Fig. 2. Phenotypic characteristics of N11/N46 SMA mice. (A) Phenotypes of N11/N46 SMA mice (SMA) and control (Ctrl: *SMN2(N11)*$^{+/-}$;*SMN2(N46)*$^{+/-}$;*Smn*$^{+/+}$) littermates during the course of the disease. Arrows indicate shortened tail and diminished or absent external ear tissue. (B) Kaplan–Meier survival curve of N11/N46 SMA mice ($n=211$). (C) Body weight evolution of N11/N46 SMA mice and control littermates between birth and PND28 (mean ± SEM; $n=2$–69 for each time point). The two-way ANOVA test indicated a significant difference (Bonferroni posttest, $P<0.001$) from day 5 onward. (D) Western blot analysis of SMN protein expression in tissues of 5 day old SMA mice [N11 SMA (N11); N46 SMA (N46) and N11/N46 SMA (N11/N46)] and control C57Bl/6N *Smn*$^{+/+}$ mice (Ctrl). Tubulin expression is shown as loading control. B, brain; SC, spinal cord; M, muscle (gastrocnemius); H, heart.

In order to investigate the behavioral problems associated with motor defects in this new SMA mouse model, several functional tests designed for new born or young mice were performed (Fig. 3). No difference between control [*SMN2(N11)*$^{+/-}$;*SMN2(N46)*$^{+/-}$;*Smn*$^{+/+}$] and N11/N46 SMA mice were observed in the acquisition of the righting reflex, neither in the percent of mice showing normal righting reflex nor in the latency to perform the test (Figs. 3A and B). In contrast N11/N46 SMA mice showed a reduced ability to perform in the negative geotaxis test compared with control mice (Figs. 3C and D). Up to PND12, most N11/N46 SMA mice failed to reorient themselves gravitationally head upwards within 60 s (scores<3) while all control mice succeeded to reorient themselves from PND8 onwards. For N11/N46 SMA mice who passed the test, the latency was significantly increased from PND9 and up to PND12. Additionally N11/N46 SMA mice showed clear behavioral defects in the tube and in the rope tests compared to controls [see Supplementary material: test tube performance at PND7 of N11/N46 SMA mouse (movie S1) and Control (movie S2); Rope test performance at PND14 of N11/N46 SMA mouse (movie S3) and Control (movie S4)]. No significant gender effect was observed in these tests (data not shown).

Electrophysiological analyses were performed with the purpose of characterizing motor and sensory nerve conduction this SMA mouse model. Compound Muscle Action Potential (CMAP) amplitude was significantly reduced in N11/N46 SMA mice compared with control littermates at 15 days of age (Table 2; up to 40% reduction). CMAP latency and duration were also significantly extended by 25% and 20%, respectively. Because sensory nerve conduction could not be evaluated due to severe tail shortening by 15 days of age, mice were submitted to the hot plate test (52°C) to detect potential sensory defects. Latency to respond to heat was increased by 117% in N11/N46 SMA mice compared with their control littermates.

Neuromuscular alterations in N11/N46 SMA mice

We then investigated whether motor defects in N11/N46 SMA mice were correlated with motor neurodegeneration. No difference in the number of lumbar (L4–L6) motor neurons was observed at PND1 while a 13% motor neuron loss was evident at PND15 compared with control *SMN2(N11)*$^{+/-}$;*SMN2(N46)*$^{+/-}$;*Smn*$^{+/+}$ littermates (Fig. 4A; 2971 ± 286 motor neurons in control and 2586 ± 179 motor neurons in N11/N46 SMA mice; mean ± SD; $P<0.05$). Similarly, a 15% decrease in the number of myelinated axons of ventral roots of the sciatic nerve (L4–L6) was evidenced at PND15 (760 ± 88 in controls and 644 ± 71 in N11/N46 SMA mice; mean ± SD; $P<0.01$), while no difference could be observed between control and N11/N46 SMA mice at PND8 (Fig. 4B). Axonal loss was also evidenced in the phrenic nerves at PND15 (-9.3%) but this difference compared to controls did not reach significance (Fig. 4C). Finally, a significant decrease in muscle fiber

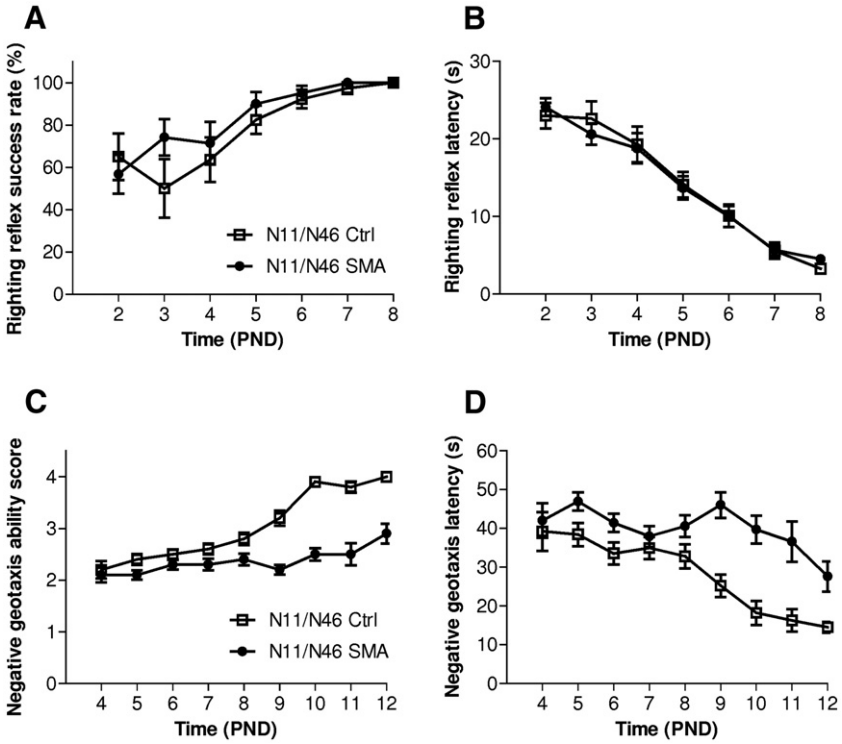

Fig. 3. Motor defects in N11/N46 SMA mice. (A, B) Righting reflex test. (A) Righting ability of N11/N46 SMA mice (filled circles) and Control: *SMN2(N11)*$^{+/-}$;*SMN2(N46)*$^{+/-}$;*Smn*$^{+/+}$ (empty squares) expressed as the percentage of the mice able to turn from their back within a 30 s period; $n = 14–39$ in each case. (B) Latency to perform the test was recorded daily starting at PND2 until PND8. No significant differences were observed between SMA and control mice in this test (two-way ANOVA, Bonferroni posttest, $P > 0.05$). (C, D) Negative geotaxis test. (C) Negative geotaxis ability of N11/N46 SMA mice (filled circles) and control mice (empty squares) was recorded daily from PND4 until PND12. Scores were assigned as described in Materials and methods; $n = 14–41$ in each case. (D) Latency to perform the test was recorded over a 60 s period. N11/N46 SMA mice showed obvious motor defects from PND9 onward compared with control mice in this test ($P < 0.001$, two-way ANOVA, Bonferroni posttest). Data represent mean ± SEM.

diameter could be noted in the gastrocnemius muscle of N11/N46 SMA mice (Figs. 4D, E).

To further characterize nerve degeneration in this new SMA mouse model, we looked for NMJ anomalies in the diaphragm and the gastrocnemius muscles at pre-symptomatic (PND1), symptomatic (PND8), and at end stages (PND15). Antibody against neurofilament M and the synaptic vesicle protein, SV2, were used to visualize axon terminals and synaptic vesicles, respectively, in the pre-synaptic region. The post-synaptic region was marked using rhodamine-conjugated alpha-bungarotoxin. In control animals, neurofilament staining showed axon terminals with homogeneous thickness and endplates with typical branched structures. The synaptic vesicle marker, SV2, was concentrated at the endplates and overlapped with neurofilament and alpha-bungarotoxin staining of the post-synaptic region. No differences in NMJ development were evident at PND1 in SMA mice either in the diaphragm (Fig. 5A) or gastrocnemius muscle (data not shown). As early as PND8, NMJs in N11/N46 SMA mice started showing neurofilament accumulation at the synaptic boutons, which appeared thick and swollen and axonal disorganization was evident in both muscles (see asterisks in Fig. 5A). This NMJ disorganization was also associated with a loss of the endplate architecture. Pre-synaptic vesicles labeled with SV2 were still present but showed a disorganized pattern as well. At PND15, NMJ disorganization was even more pronounced and denervated endplates could be observed. In this case the neurofilament and the synaptic vesicle staining in the synapses were no longer present. Only alpha-bungarotoxin labeled post-synaptic acetylcholine receptors were visible, appearing as vacant endplates (see arrows in Fig. 5B). Finally, at PND15, more denervated synapses were observed in diaphragm compared to gastrocnemius muscle although no exhaustive quantification was performed. Taken together, these data indicated a progressive neuromuscular degeneration in N11/N46 SMA mice, correlating with muscle atrophy.

Table 2
Electromyographical and sensory defects in N11/N46 SMA mice. Compound Muscle Action Potential (CMAP) was measured in the gastrocnemius muscle of 15 day old N11/N46 SMA mice (*Smn*$^{-/-}$; $n = 10$) and control littermates: *SMN2(N11)*$^{+/-}$;*SMN2(N46)*$^{+/-}$; *Smn*$^{+/+}$ (*Smn*$^{+/+}$; $n = 30$) and *SMN2(N11)*$^{+/-}$;*SMN2(N46)*$^{+/-}$;*Smn*$^{+/-}$ (*Smn*$^{+/-}$; $n = 40$). Hot plate threshold was adjusted to 52 °C. Latency for the animal to react by moving or licking their paw was measured. Data are means ± SEM. *P* values, SMA mice as compared to control *Smn*$^{+/+}$ group, one-way ANOVA.

N11/N46 mice	EMG			Hot plate
	Amplitude (mV)	Latency (ms)	Duration (ms)	Latency (ms)
Smn$^{+/+}$	19.82 ± 0.97	0.81 ± 0.02	2.70 ± 0.10	7.10 ± 0.52
Smn$^{+/-}$	21.38 ± 1.28	0.83 ± 0.03	2.78 ± 0.08	7.28 ± 0.48
Smn$^{-/-}$ (SMA)	12.48 ± 2.32	0.99 ± 0.07	3.21 ± 0.26	15.82 ± 1.15
P value	<0.001	<0.005	<0.05	<0.001

Early NMJs defects in diaphragm were associated with respiratory impairments in SMA mice

To test whether early appearance of NMJ abnormalities in N11/N46 SMA mice, particularly in diaphragm, could result in respiratory defects, the breathing pattern of SMA mice and their control littermates was studied under normoxic and hypoxic conditions using non-invasive plethysmography. Under normoxic conditions, no significant differences in breathing variables were observed between groups at PND1 (Fig. 6A). However the maturation of breathing variables measured on PND7 was impaired in N11/N46 SMA pups (Fig. 6B). Indeed, ventilation (V_E) was significantly smaller in SMA mice on PND7 compared to control mice (Fig. 6C). Similarly, breath duration (T_{TOT}) was significantly longer in SMA mice compared to control littermates indicating decreased respiratory rate in SMA mice

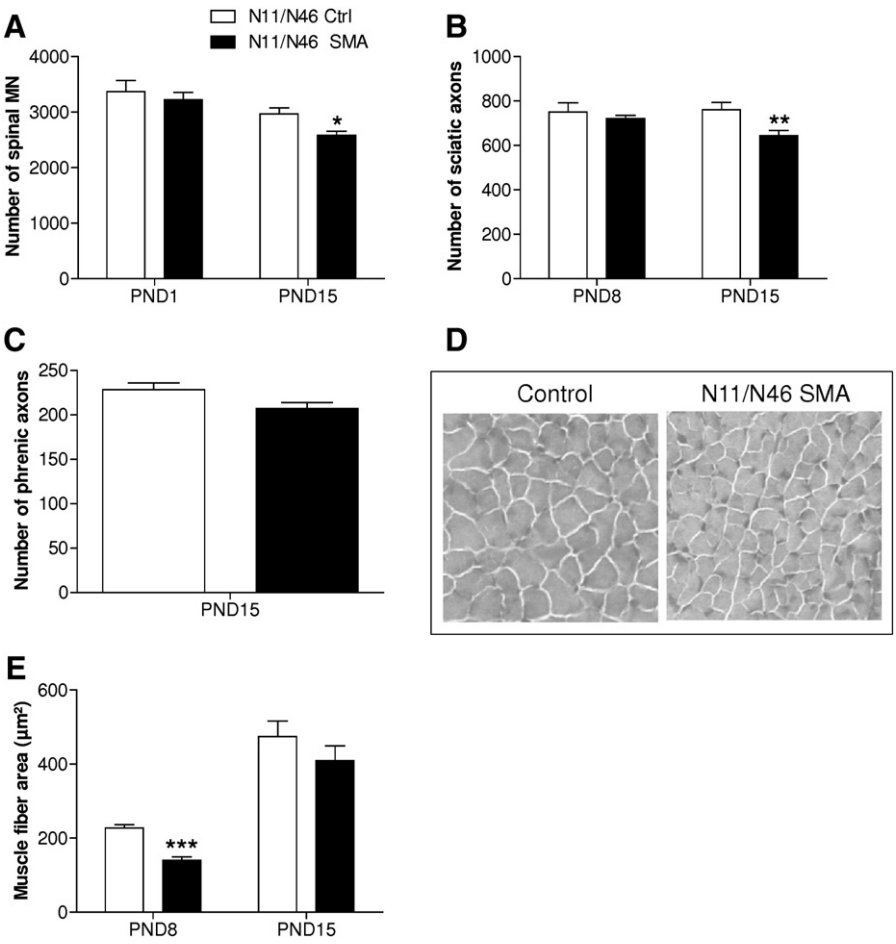

Fig. 4. Histological signs of progressive neuromuscular degeneration in N11/N46 SMA mice. (A) Quantification of lumbar (L4–L6) motor neurons in N11/N46 SMA mice and control (Ctrl: *SMN2(N11)*$^{+/-}$;*SMN2(N46)*$^{+/-}$;*Smn*$^{+/+}$) littermates at PND1 and at PND15 ($n=5$–7 mice/genotype/age). (B) Number of myelinated axons in ventral roots of the sciatic nerve at PND8 and at PND15 ($n=5$–10 mice/genotype/age). (C). Number of axons in the phrenic nerve counted at PND15 ($n=6$–8 mice/genotype). (D) Representative images of transverse sections through the gastrocnemius muscle showing fiber atrophy in N11/N46 SMA mice at PND15 compared to control. (E) Muscle fiber area at PND8 and at PND15 ($n=5$–12 mice/genotype/age). Data represent mean ± SEM. *$P<0.05$; **$P<0.01$; and ***$P<0.001$, unpaired *t*-test.

on PND7 (Fig. 6C). Consistent with the decreased maturation in breathing variables, apnea duration, which normally decreased between PND1 and PND7 (see control littermates), remained significantly higher in SMA mice at PND7 compared to control littermates (Fig. 6C). Importantly, no difference was observed in potential confounding factors, body temperature and cardiac frequency, between genotype groups at either age (Supplementary Table 1). Finally all mice increased ventilation in response to hypoxia on PND1 and PND7 (Figs. 6A, B). The percentage increase from baseline was not different between genotype groups (Fig. 7). Movement durations and ultrasonic vocalizations, which are two markers of the behavioral response to hypoxia, were not significantly different between genotype groups (Supplementary Fig. 2).

Discussion

We report here the establishment of a new SMA mouse carrying three copies of *SMN2* on a null *Smn* background. Though indistinguishable from normal littermates in the first 4 days after birth, these mice rapidly developed muscle weakness and motor defects along with diminished weight gain. At PND14 (median survival), motor neuron and axonal loss were evident, correlated with a reduction in compound muscle action potential amplitude, and in nerve conduction. Defects in neuromuscular junction maturation were observed as early as PND8 in the diaphragm. Importantly, we report for the first time marked differences in breathing patterns in SMA pups at PND7 with smaller ventilation volume, longer breath duration and greater apnea frequency and duration. Such defects could underlie the premature death of SMA mice.

Neurodegenerative process in SMA mice

Because previously reported SMA mouse models were severely affected and died prematurely (Hsieh-Li et al., 2000; Monani et al., 2000), we attempted to develop a slower progressing SMA phenotype by manipulating only the number of *SMN2* copies. On a pure C57BL/6N background, we show that two copies of *SMN2* poorly rescued murine *Smn* gene deletion (N11 SMA mice) while four copies largely rescued them (N46 SMA mice). Interestingly, by intercrossing these two lines we were able to generate *Smn* null mice harboring three copies of *SMN2* (N11/N46 SMA mice). As expected, these mice displayed delayed disease onset, slower disease progression and longer survival compared with *Smn* null mice harboring two *SMN2* copies (median survival improved by about 200%, from 6 to 14 days). Delay in body weight gain at around 7 days of age was the first evidence of a degenerative phenotype. At PND9, N11/N46 SMA mice had decreased physical activity, slowed movement and demonstrated significant motor defects in the geotaxis test and in the tube test (Supplementary material). Similar defects were reported as early as PND4 in *SMNΔ7*;*SMN2*;*Smn*$^{-/-}$ mice (SMNΔ7 SMA mice) (Butchbach et al., 2007; El-Khodor et al., 2008). Interestingly, we did not observe impairments in righting reflex ability in N11/N46 SMA mice while

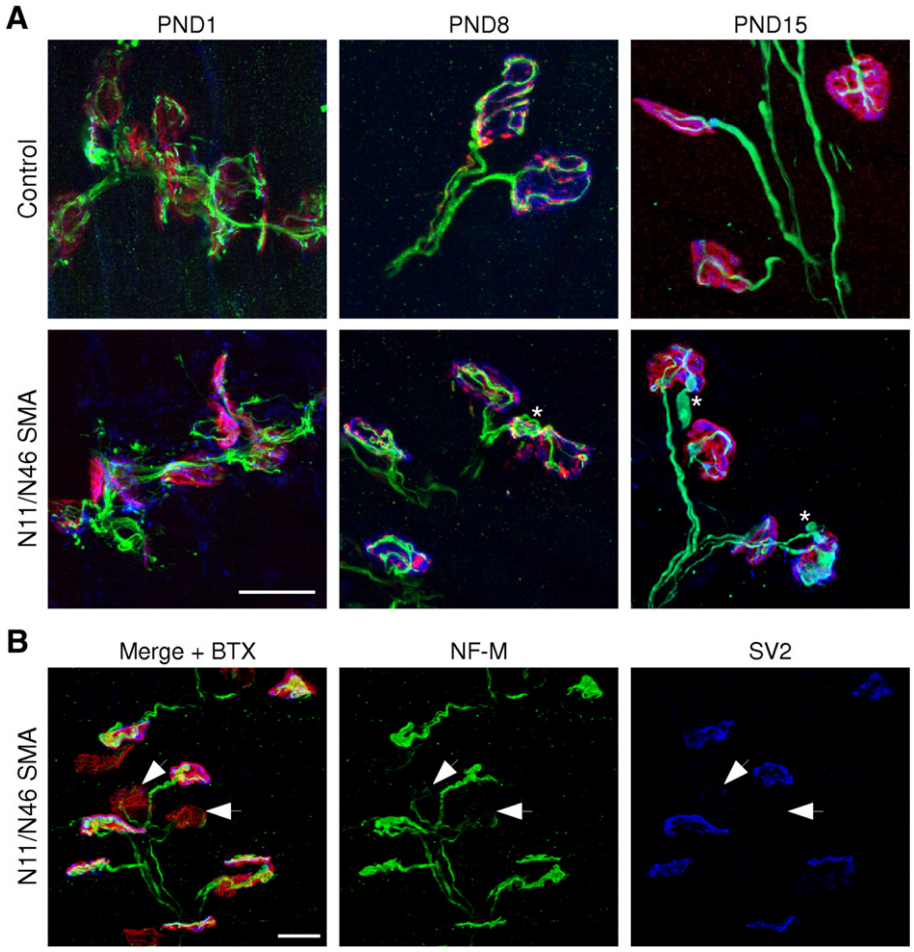

Fig. 5. Pre- and post-synaptic NMJ defects in N11/N46 SMA mice. (A) Representative images of diaphragmatic NMJs in N11/N46 SMA mice and control (Ctrl: *SMN2(N11)*$^{+/-}$;*SMN2(N46)*$^{+/-}$;*Smn*$^{+/+}$ or *SMN2(N11)*$^{+/-}$;*SMN2(N46)*$^{+/-}$;*Smn*$^{+/-}$) littermates at different ages: PND1, PND8 and PND15. Green: Neurofilament M. Blue: synaptic vesicle marker, SV2. Red: rhodamine-alpha-bungarotoxin to mark the post-synaptic acetylcholine receptors. At PND8 motor axons are already disorganized with accumulation of neurofilament at the synaptic terminal (asterisks), which is even more evident at PND15. (B) Representative images of diaphragmatic NMJs of a PND15 N11/N46 SMA mouse with a more severe phenotype. Arrows indicate sites of denervation as evidenced by the absence of synaptic vesicle labeling.

righting ability is strongly compromised in SMNΔ7 SMA mice (Butchbach et al., 2007; El-Khodor et al., 2008; Kariya et al., 2008). This clearly suggests that N11/N46 SMA mice are less severely affected than previously described SMNΔ7 SMA mice (see Table 3 for a comparison of the two models).

The onset of neurodegeneration was also slowed in N11/N46 SMA mice. Loss of lumbar motor neurons and motor axons in lumbar ventral roots was evident only at a late stage (around 15% reduction at PND15). This result is in agreement with previous observations indicating that timing of motor neuron loss is related to disease severity [PND3 in severe *SMN2*;*Smn*$^{-/-}$ (Type I); PND9 in *SMNΔ7*;*SMN2*;*Smn*$^{-/-}$; >3 months in *SMNA2G*;*SMN2*;*Smn*$^{-/-}$ (Type III)]. The earliest defects were observed at the NMJ with the appearance of pre-synaptic neurofilament accumulation and empty NMJs both in diaphragm and in gastrocnemius muscles as early as PND8 while no differences between control and SMA mice were observed at PND1. Similar early morphological changes in synapses were described in severe SMA mice (Kariya et al., 2008; McGovern et al., 2008). It was hypothesized that these defects resulted from impairment in post-natal maturation of NMJs. In agreement with this, morphological analysis of the gastrocnemius muscle revealed the presence of muscle atrophy with drastically reduced myofiber diameter but no sign of neurogenic atrophy was observed suggesting that denervation/reinnervation processes did not have time to occur. It should be noted that SMN protein levels were particularly low in skeletal and heart muscles compared to relatively spared levels in CNS tissues of N11/N46 SMA mice. Thus we may also consider a specific muscle defect at post-synaptic level. Importantly, these structural abnormalities of NMJ underlie the drastic reduction in motor nerve conduction velocity and amplitude (-25% and -40%, respectively) that probably account for motor deficits. To explore potential defects in sensory neurons in N11/N46 SMA mice as was suggested for severe SMA mice (Jablonka et al., 2006), we submitted PND15 mice to the hot plate test. Paw withdrawal latency was increased by 117% in SMA mice suggesting that sensory functions could be impaired at that age. However, we cannot exclude that such altered response may be a consequence of impaired motor function. Further analysis of sensory nerve ending footpads will be required to reach this conclusion.

Respiratory defects in SMA mice

Individuals with SMA develop inspiratory and expiratory respiratory muscle weakness leading to progressive respiratory failure. No obvious changes in respiratory movements of the thorax and abdomen were observed in SMNΔ7 SMA mice suggesting that respiratory rate was not impaired (El-Khodor et al., 2008). However the severity of the disease progression in this SMA mouse model precluded any reliable investigation of such defects. Here, the extended survival of the N11/N46 SMA mice allowed us to quantitatively measure respiratory rate, ventilation volume and apneas using non-invasive flow barometric plethysmography. We found that the breathing pattern in N11/N46 SMA pups was normal

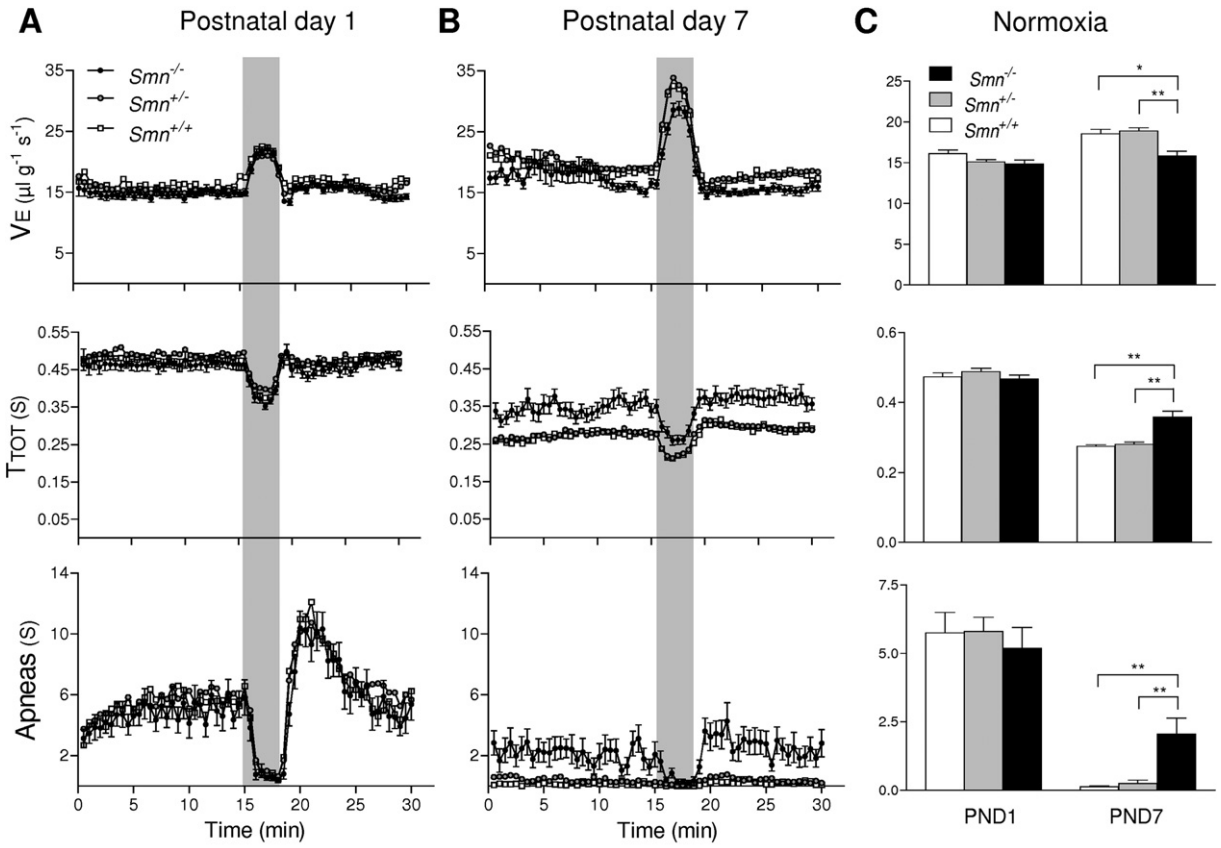

Fig. 6. Breathing variables in N11/N46 SMA mice. (A, B) Ventilation (V_E), breath duration (T_{TOT}), and apnea were recorded during normoxia and in response to hypoxia (10% O_2, shaded areas) in N11/N46 SMA mice ($Smn^{-/-}$; black circles, $n=18$) and control littermates ($Smn^{+/-}$; gray circles, $n=52$ and $Smn^{+/+}$; empty square, $n=21$) on PND1 (A) and PND7 (B). (C) Mean values during the 3-min of normoxia preceding the hypoxic period. On PND1, breathing variables were indistinguishable between groups in normoxia. In contrast on PND7, normoxic ventilation was smaller in SMA pups while T_{TOT} and apnea duration were significantly longer in SMA compared to control mice. V_E and T_{TOT} were averaged over consecutive 30-s periods. Total apnea duration was calculated over successive 30-s periods. Values are means ± SEM. *$P<0.05$; **$P<0.001$, one-way ANOVA.

on PND1 but was markedly abnormal on PND7 compared to control littermates. Indeed SMA mice displayed smaller ventilation levels, compared to control littermates, due to their longer breath durations (i.e. lower breathing frequency). This difference was accompanied by more frequent and longer apnea durations. These results suggest impairment in ventilatory maturation in SMA mice from PND1 to PND7. In SMA patients, chronic respiratory failure mostly results from intercostal muscle paralysis while the diaphragm is thought to be relatively spared since breathing is almost entirely diaphragmatic (Dubowitz, 1978). However Monani's group recently provided evidence of profound structural defects of the NMJ in diaphragmatic muscle of type I SMA patients (Kariya et al., 2008). Here we show that the appearance of NMJ defects in the diaphragm paralleled ventilatory impairment; thus, we may hypothesize that diaphragm mis-innervation plays a causative role in impaired respiration. Evidence of intercostal muscles denervation was also reported in other SMA mice (Kariya et al., 2008; McGovern et al., 2008) and this could also contribute to the respiratory defects we observe in N11/N46 SMA mice, although we did not investigate this point. Whether breathing defects account for the premature death of SMA mice as for SMA patients remains difficult to ascertain. Indeed respiratory impairments may affect general status and, along with motor impairment, compromise the ability to compete with littermates for access to nipples and suckle, thus leading to undernourishment and growth retardation. Disruption of coordination between respiration and swallowing may also compromise milk intake and cause growth retardation. Thus both respiratory and nutritional impairments may be implicated in the early death of SMA mice.

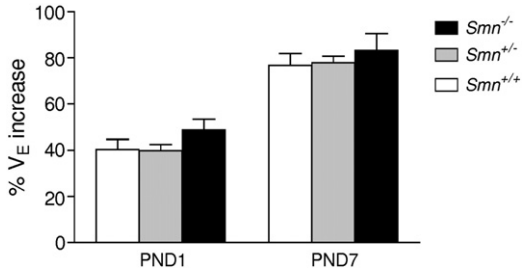

Fig. 7. Ventilatory response to hypoxia. Ventilatory response to hypoxia was expressed as the percentage V_E change relative to baseline V_E. The percentage increases from baseline values were not significantly different between genotype groups on PND1 and PND7 ($P>0.05$, one-way ANOVA). Values are means ± SEM.

Future of SMA modeling in mice

Altogether, our results demonstrate that N11/N46 SMA mice recapitulate neuromuscular defects and breathing disorders observed in severe forms of SMA. The delayed disease onset and progression we report in this model, along with a well defined genetic characterization (pure genetic background, precise *SMN2* copy number, and defined transgene localization) will make these mice an important tool in deciphering the role of *SMN2* as a modifier gene for SMA and in evaluating new therapeutics. As one additional copy of *SMN2* fully rescued the phenotype, it appears unlikely that a milder phenotype can be produced by manipulating *SMN2* copy number alone. Here, inversing the breeding had a slight but significant effect on lifespan with a greater percentage of animals "escaping" and surviving into

Table 3
Comparison of neuromuscular degenerative phenotype in SMNΔ7 and N11/N46 SMA mice.

	SMNΔ7 SMA mice	N11/N46 SMA mice
Gene defect	*SMN*$^{\Delta7/\ \Delta7}$;*SMN2*$^{+/+}$;*Smn*$^{-/-}$	*SMN2(N11)*$^{+/+}$;*SMN2(N46)*$^{+/+}$;*Smn*$^{-/-}$
Background (fully congenic)	FVB/N	C57BL/6N
Locomotor activity	Righting defect at PND2 Geotaxis defect at PND4	No righting defect Geotaxis defect at PND9
Body weight peak	PND8	PND18
NMJ defects	Impaired post-natal maturation at PND2 in diaphragm, PND8 in gastrocnemius	Marked abnormal appearance at PND8 in diaphragm and in gastrocnemius
Motor axon loss	-30% at PND14 in phrenic nerves and C4-ventral roots (preferentially large caliber axons>3.5 μm); No significant loss in L4-ventral roots	-15% in lumbar ventral roots at PND15; -9% in phrenic nerve at same age
Motor neuron loss	-19% at PND9 (L3–L6)	-13% at PND15 (L4–L6)
Mean survival (median survival)	11.4 ± 0.4 days (11 days)	15.2 ± 0.4 days (14 days)

Data from Kariya et al. (2008) reporting fully congenic FVB/N mice; may differ from initial description on mixed genetic background.

adulthood with a normal lifespan despite the deleterious effects on tail, ear and hind feet, suggesting that epigenetic factors may modify disease progression and survival. *SMN* gene expression is influenced by DNA methylation and acetylation as demonstrated by the effect of HDAC inhibitors (Kernochan et al., 2005). We could speculate that gender may influence expression of some genes involved in the regulation of *SMN* transcription, splicing or translation. Other possibilities include gender controlled modifier gene(s) as previously shown for the plastin 3 gene (Oprea et al., 2008). In the future, we might expect that breeding strategies using these mice may allow identification of other genes that modify SMA severity and eventually produce less severely affected SMA mice.

Acknowledgments

We thank Drs. Christine DiDonato, Serge Braun and Chris Henderson for helpful discussion during the project. We are grateful to Boris Matrot for designing the phenotyping systems for newborn mice. The skillful assistance of Virginie Latyszenok, Michel Bruno and Danielle Depetris was highly appreciated. This work was supported by the Association Française contre les Myopathies (AFM); the German Research Foundation [SFB 581 to M.S., 945/12-3 to B.W.]; the Center for Molecular Medicine, University of Cologne [CMMC-D5 to B.W.]; and the EU 6th Framework Program [NeuroNE network of excellence grant to S.B.].

Appendix A. Supplementary data

Supplementary data associated with this article can be found, in the online version, at doi:10.1016/j.nbd.2010.01.006.

References

Burghes, A.H., 1997. When is a deletion not a deletion? When it is converted. Am. J. Hum. Genet. 61, 9–15.
Burghes, A.H., Beattie, C.E., 2009. Spinal muscular atrophy: why do low levels of survival motor neuron protein make motor neurons sick? Nat. Rev. Neurosci. 10, 597–609.
Bussaglia, E., Clermont, O., Tizzano, E., Lefebvre, S., Burglen, L., Cruaud, C., Urtizberea, J.A., Colomer, J., Munnich, A., Baiget, M., et al., 1995. A frame-shift deletion in the survival motor neuron gene in Spanish spinal muscular atrophy patients. Nat. Genet. 11, 335–337.
Butchbach, M.E., Edwards, J.D., Burghes, A.H., 2007. Abnormal motor phenotype in the SMNDelta7 mouse model of spinal muscular atrophy. Neurobiol. Dis. 27, 207–219.
Carrel, T.L., McWhorter, M.L., Workman, E., Zhang, H., Wolstencroft, E.C., Lorson, C., Bassell, G.J., Burghes, A.H., Beattie, C.E., 2006. Survival motor neuron function in motor axons is independent of functions required for small nuclear ribonucleoprotein biogenesis. J. Neurosci. 26, 11014–11022.
Cifuentes-Diaz, C., Nicole, S., Velasco, M.E., Borra-Cebrian, C., Panozzo, C., Frugier, T., Millet, G., Roblot, N., Joshi, V., Melki, J., 2002. Neurofilament accumulation at the motor endplate and lack of axonal sprouting in a spinal muscular atrophy mouse model. Hum. Mol. Genet. 11, 1439–1447.
Coovert, D.D., Le, T.T., McAndrew, P.E., Strasswimmer, J., Crawford, T.O., Mendell, J.R., Coulson, S.E., Androphy, E.J., Prior, T.W., Burghes, A.H., 1997. The survival motor neuron protein in spinal muscular atrophy. Hum. Mol. Genet. 6, 1205–1214.
Crawford, T.O., Pardo, C.A., 1996. The neurobiology of childhood spinal muscular atrophy. Neurobiol. Dis. 3, 97–110.
Dauger, S., Durand, E., Cohen, G., Lagercrantz, H., Changeux, J.P., Gaultier, C., Gallego, J., 2004. Control of breathing in newborn mice lacking the beta-2 nAChR subunit. Acta Physiol. Scand. 182, 205–212.
DiDonato, C.J., Chen, X.N., Noya, D., Korenberg, J.R., Nadeau, J.H., Simard, L.R., 1997. Cloning, characterization, and copy number of the murine survival motor neuron gene: homolog of the spinal muscular atrophy-determining gene. Genome Res. 7, 339–352.
Dubowitz, V., 1978. Muscle disorders in childhood. Major Probl. Clin. Pediatr. 16, 1–282 iii–xiii.
El-Khodor, B.F., Edgar, N., Chen, A., Winberg, M.L., Joyce, C., Brunner, D., Suarez-Farinas, M., Heyes, M.P., 2008. Identification of a battery of tests for drug candidate evaluation in the SMNDelta7 neonate model of spinal muscular atrophy. Exp. Neurol. 212, 29–43.
Feldkotter, M., Schwarzer, V., Wirth, R., Wienker, T.F., Wirth, B., 2002. Quantitative analyses of SMN1 and SMN2 based on real-time lightCycler PCR: fast and highly reliable carrier testing and prediction of severity of spinal muscular atrophy. Am. J. Hum. Genet. 70, 358–368.
Frugier, T., Tiziano, F.D., Cifuentes-Diaz, C., Miniou, P., Roblot, N., Dierich, A., Le Meur, M., Melki, J., 2000. Nuclear targeting defect of SMN lacking the C-terminus in a mouse model of spinal muscular atrophy. Hum. Mol. Genet. 9, 849–858.
Hendrickson, B.C., Donohoe, C., Akmaev, V.R., Sugarman, E.A., Labrousse, P., Bogus-lavskiy, L., Flynn, K., Rohlfs, E.M., Walker, A., Allitto, B., Sears, C., Scholl, T., 2009. Differences in SMN1 allele frequencies among ethnic groups within North America. J. Med. Genet. 46, 641–644.
Hsieh-Li, H.M., Chang, J.G., Jong, Y.J., Wu, M.H., Wang, N.M., Tsai, C.H., Li, H., 2000. A mouse model for spinal muscular atrophy. Nat. Genet. 24, 66–70.
Jablonka, S., Karle, K., Sandner, B., Andreassi, C., von Au, K., Sendtner, M., 2006. Distinct and overlapping alterations in motor and sensory neurons in a mouse model of spinal muscular atrophy. Hum. Mol. Genet. 15, 511–518.
Kariya, S., Park, G.H., Maeno-Hikichi, Y., Leykekhman, O., Lutz, C., Arkovitz, M.S., Landmesser, L.T., Monani, U.R., 2008. Reduced SMN protein impairs maturation of the neuromuscular junctions in mouse models of spinal muscular atrophy. Hum. Mol. Genet. 17, 2552–2569.
Kernochan, L.E., Russo, M.L., Woodling, N.S., Huynh, T.N., Avila, A.M., Fischbeck, K.H., Sumner, C.J., 2005. The role of histone acetylation in SMN gene expression. Hum. Mol. Genet. 14, 1171–1182.
Le, T.T., Coovert, D.D., Monani, U.R., Morris, G.E., Burghes, A.H., 2000. The survival motor neuron (SMN) protein: effect of exon loss and mutation on protein localization. Neurogenetics 3, 7–16.
Le, T.T., Pham, L.T., Butchbach, M.E., Zhang, H.L., Monani, U.R., Coovert, D.D., Gavrilina, T.O., Xing, L., Bassell, G.J., Burghes, A.H., 2005. SMNDelta7, the major product of the centromeric survival motor neuron (SMN2) gene, extends survival in mice with spinal muscular atrophy and associates with full-length SMN. Hum. Mol. Genet. 14, 845–857.
Lefebvre, S., Burglen, L., Reboullet, S., Clermont, O., Burlet, P., Viollet, L., Benichou, B., Cruaud, C., Millasseau, P., Zeviani, M., et al., 1995. Identification and characterization of a spinal muscular atrophy-determining gene. Cell 80, 155–165.
Lefebvre, S., Burlet, P., Liu, Q., Bertrandy, S., Clermont, O., Munnich, A., Dreyfuss, G., Melki, J., 1997. Correlation between severity and SMN protein level in spinal muscular atrophy. Nat. Genet. 16, 265–269.
Liu, Q., Dreyfuss, G., 1996. A novel nuclear structure containing the survival of motor neurons protein. EMBO J. 15, 3555–3565.
Liu, Q., Fischer, U., Wang, F., Dreyfuss, G., 1997. The spinal muscular atrophy disease gene product, SMN, and its associated protein SIP1 are in a complex with spiceosomal snRNP proteins. Cell 90, 1013–1021.
Lobsiger, C.S., Boillee, S., McAlonis-Downes, M., Khan, A.M., Feltri, M.L., Yamanaka, K., Cleveland, D.W., 2009. Schwann cells expressing dismutase active mutant SOD1 unexpectedly slow disease progression in ALS mice. Proc. Natl. Acad. Sci. U. S. A. 106, 4465–4470.
Lorson, C.L., Androphy, E.J., 2000. An exonic enhancer is required for inclusion of an essential exon in the SMA-determining gene SMN. Hum. Mol. Genet. 9, 259–265.
Lorson, C.L., Strasswimmer, J., Yao, J.M., Baleja, J.D., Hahnen, E., Wirth, B., Le, T., Burghes, A.H., Androphy, E.J., 1998. SMN oligomerization defect correlates with spinal muscular atrophy severity. Nat. Genet. 19, 63–66.

Lorson, C.L., Hahnen, E., Androphy, E.J., Wirth, B., 1999. A single nucleotide in the SMN gene regulates splicing and is responsible for spinal muscular atrophy. Proc. Natl. Acad. Sci. U. S. A. 96, 6307–6311.

Matrot, B., Durand, E., Dauger, S., Vardon, G., Gaultier, C., Gallego, J., 2005. Automatic classification of activity and apneas using whole body plethysmography in newborn mice. J. Appl. Physiol. 98, 365–370.

McAndrew, P.E., Parsons, D.W., Simard, L.R., Rochette, C., Ray, P.N., Mendell, J.R., Prior, T.W., Burghes, A.H., 1997. Identification of proximal spinal muscular atrophy carriers and patients by analysis of SMNT and SMNC gene copy number. Am. J. Hum. Genet. 60, 1411–1422.

McGovern, V.L., Gavrilina, T.O., Beattie, C.E., Burghes, A.H., 2008. Embryonic motor axon development in the severe SMA mouse. Hum. Mol. Genet. 17, 2900–2909.

Monani, U.R., Lorson, C.L., Parsons, D.W., Prior, T.W., Androphy, E.J., Burghes, A.H.M., McPherson, J.D., 1999. A single nucleotide difference that alters splicing patterns distinguishes the SMA gene SMN1 from the copy gene SMN2. Hum. Mol. Genet. 8, 1177–1183.

Monani, U.R., Sendtner, M., Coovert, D.D., Parsons, D.W., Andreassi, C., Le, T.T., Jablonka, S., Schrank, B., Rossol, W., Prior, T.W., Morris, G.E., Burghes, A.H., 2000. The human centromeric survival motor neuron gene (SMN2) rescues embryonic lethality in Smn(-/-) mice and results in a mouse with spinal muscular atrophy. Hum. Mol. Genet. 9, 333–339.

Monani, U.R., Pastore, M.T., Gavrilina, T.O., Jablonka, S., Le, T.T., Andreassi, C., DiCocco, J.M., Lorson, C., Androphy, E.J., Sendtner, M., Podell, M., Burghes, A.H., 2003. A transgene carrying an A2G missense mutation in the SMN gene modulates phenotypic severity in mice with severe (type I) spinal muscular atrophy. J. Cell. Biol. 160, 41–52.

Oprea, G.E., Krober, S., McWhorter, M.L., Rossoll, W., Muller, S., Krawczak, M., Bassell, G.J., Beattie, C.E., Wirth, B., 2008. Plastin 3 is a protective modifier of autosomal recessive spinal muscular atrophy. Science 320, 524–527.

Pearn, J., 1978. Incidence, prevalence and gene frequency studies of chronic childhood spinal muscular atrophy. J. Med. Genet. 15, 409–413.

Pellizzoni, L., Kataoka, N., Charroux, B., Dreyfuss, G., 1998. A novel function of SMN, the spinal muscular atrophy disease gene product, in pre-mRNA splicing. Cell 95, 615–624.

Pellizzoni, L., Yong, J., Dreyfuss, G., 2002. Essential role for the SMN complex in the specificity of snRNP assembly. Science 298, 1775–1779.

Ramanantsoa, N., Vaubourg, V., Dauger, S., Matrot, B., Vardon, G., Chettouh, Z., Gaultier, C., Goridis, C., Gallego, J., 2006. Ventilatory response to hyperoxia in newborn mice heterozygous for the transcription factor Phox2b. Am. J. Physiol. Regul. Integr. Comp. Physiol. 290, R1691–R1696.

Rossoll, W., Jablonka, S., Andreassi, C., Kroning, A.K., Karle, K., Monani, U.R., Sendtner, M., 2003. Smn, the spinal muscular atrophy-determining gene product, modulates axon growth and localization of beta-actin mRNA in growth cones of motoneurons. J. Cell. Biol. 163, 801–812.

Sawnani, H., Jackson, T., Murphy, T., Beckerman, R., Simakajornboon, N., 2004. The effect of maternal smoking on respiratory and arousal patterns in preterm infants during sleep. Am. J. Respir. Crit. Care Med. 169, 733–738.

Scheffer, H., Cobben, J.M., Matthijs, G., Wirth, B., 2001. Best practice guidelines for molecular analysis in spinal muscular atrophy. Eur. J. Hum. Genet. 9, 484–491.

Schrank, B., Götz, R., Gunnersen, J.M., Ure, J.M., Toyka, K.V., Smith, A.G., Sendtner, M., 1997. The inactivation of the survival motor neuron gene, a candidate gene for human spinal muscular atrophy, leads to massive cell death in early mouse embryos. Proc. Natl. Acad. Sci. U.S.A. 94, 9920–9925.

Schroth, M.K., 2009. Special considerations in the respiratory management of spinal muscular atrophy. Pediatrics 123 (Suppl 4), S245–S249.

Tsai, L.K., Tsai, M.S., Lin, T.B., Hwu, W.L., Li, H., 2006. Establishing a standardized therapeutic testing protocol for spinal muscular atrophy. Neurobiol. Dis. 24, 286–295.

Tsai, L.K., Tsai, M.S., Ting, C.H., Li, H., 2008a. Multiple therapeutic effects of valproic acid in spinal muscular atrophy model mice. J. Mol. Med. 86, 1243–1254.

Tsai, L.K., Tsai, M.S., Ting, C.H., Wang, S.H., Li, H., 2008b. Restoring Bcl-x(L) levels benefits a mouse model of spinal muscular atrophy. Neurobiol. Dis. 31, 361–367.

Viollet, L., Bertrandy, S., Bueno Brunialti, A.L., Lefebvre, S., Burlet, P., Clermont, O., Cruaud, C., Guenet, J.L., Munnich, A., Melki, J., 1997. cDNA isolation, expression, and chromosomal localization of the mouse survival motor neuron gene (Smn). Genomics 40, 185–188.

Zhang, H.L., Pan, F., Hong, D., Shenoy, S.M., Singer, R.H., Bassell, G.J., 2003. Active transport of the survival motor neuron protein and the role of exon-7 in cytoplasmic localization. J. Neurosci. 23, 6627–6637.